Hypoxia-inducible-factors differentially contribute to clinical disease and the control of viral replication during RSV infection

Dorothea R. Morris[1,2,3], Yue Qu[3], Yava L. Jones-Hall[4], Tianshuang Liu[3], Teodora Ivanciuc[3], Roberto P. Garofalo[1,3], Antonella Casola[1,3,*]

[1]Department of Microbiology & Immunology, The University of Texas Medical Branch, Galveston, TX, USA

[2]School of Population & Public Health, The University of Texas Medical Branch, Galveston, TX, USA

[3]Department of Pediatrics, The University of Texas Medical Branch, Galveston, TX, USA

[4]School of Veterinary Medicine and Biomedical Science, Texas A&M University, College Station, TX, USA

*** Correspondence:**
Antonella Casola
ancasola@utmb.edu

Keywords: RSV, respiratory syncytial virus, hypoxia-inducible-factors, HIF-1a, HIF-2a, PX478, PT2385

1 Abstract

Hypoxia-inducible-factors (HIF) are transcription factors that regulate cellular adaptation to hypoxic conditions, enabling cells to survive in low-oxygen environments. Viruses have evolved to stabilize this pathway to promote successful viral infection, therefore modulation of HIFs could represent a novel antiviral strategy. In previous *in vitro* studies, we found that respiratory syncytial virus (RSV), a leading cause of respiratory illness, stabilizes HIFs under normoxic conditions, with inhibition of HIF-1α resulting in reduced viral replication. Despite several HIF modulating compounds being tested/approved for use in other non-infectious models, little is known about their efficacy against respiratory viruses using relevant animal models. This study aimed to characterize the disease modulating properties and antiviral potential of anti-HIF-1α (PX478) and anti-HIF-2α (PT2385) in RSV-infected BALB/c mice. We found that inhibition of HIF-1α worsen clinical disease parameters,

while simultaneously improving airway function. Additionally, anti-HIF-1α results in significantly reduced viral titer at early and peak time points of RSV replication, followed by a loss in viral clearance when given every day, but not every-other-day. In contrast, inhibition of HIF-2α was associated with improved clinical parameters, with no changes in airway function, and amelioration of interstitial pneumonia. Furthermore, anti-HIF-2α reduced early and peak lung viral replication, with no impairment of viral clearance. Analysis of lung cells found significant modification in the T cell compartment that correlated with changes in lung pathology and viral titers in response to each HIF inhibitor administration. These data underscore the complex role of HIFs in RSV infection and highlight the need for careful therapeutic consideration.

2 Introduction

Respiratory syncytial virus (RSV) is a prominent cause of respiratory infections among infants, young children, and the elderly. Each year, there are an estimated 33 million infections and 150,000 deaths [1]. Infection with RSV often results in damage to the airways and a dysregulated immune response that contributes to the development of bronchiolitis and pneumonia. Although prophylactic treatment and vaccines licensed for use in pregnant women and elderly patients are available, there are no therapeutic agents licensed for the treatment of RSV infection [2-4]. Furthering our understanding of the pathology of RSV is important to protecting these vulnerable populations.

As an obligate intracellular pathogen, viruses rely on host cell machinery to establish productive infections. Many viruses have been shown to modify cellular metabolism to achieve virion assembly by increasing sources of energy and generating pools of free nucleotides, amino acids, lipid materials, and glycoproteins [5]. One mechanism frequently associated with this is the manipulation of the hypoxia-inducible-factor (HIF) pathway. As the gatekeeper to a diverse biological network, the use of the HIF pathway allows many viruses to create a cellular environment that favors viral replication, persistence, and immune evasion. The manipulation of this pathway has been observed with several

DNA and RNA viruses, even under oxygen-rich conditions [6, 7]. The significance of HIF in cancer pathology has led much of the existing literature to focus on viruses known to induce tumor formation as part of their pathogenic mechanism [6, 7]. Surprisingly, limited research has explored the clinical manifestations and pathological contributions of HIFs to viral respiratory infections [6-9].

HIFs are transcription factors that regulate the expression of a wide range of target genes in response to low oxygen levels [10]. These target genes have crucial roles in diverse biological processes, enabling cells to adapt and survive under hypoxic conditions. The HIF complex is a heterodimer consisting of an inducible α subunit (HIF-1α, HIF-2α, or HIF-3α) and a constitutively expressed β subunit (HIF-1β) [11]. While there is overlap in their functionality, the HIF-α isoforms also exhibit distinct transcriptional regulation in response to hypoxia and disease states [12-14]. HIF-1α is the most extensively studied isoform of the HIF family. Expressed in nearly all cell types, HIF-1α is the master regulator of cellular and systemic responses to hypoxia. Genes activated by HIF-1α modify a broad range of processes including energy metabolism, angiogenesis, epithelial-mesenchymal transition (EMT), and immune cell regulation [12, 14]. HIF-2α, though not as thoroughly described as HIF-1, has been shown to exhibit a more limited distribution; predominately expressed in specific organs such as the kidney, liver, and lung. Genes upregulated by HIF-2α in models of cancer and of non-infectious tissue repair are primarily involved in erythropoiesis, vascular development, and iron metabolism [14]. HIF-3α is the most recent of the HIF isoforms to be identified. Because of this, the precise distribution and function of HIF-3α is still being investigated.

Our laboratory recently found that RSV stabilizes both HIF-1α and HIF-2α in primary small airway epithelial cells and diverts core metabolic activity towards the glycolytic pathway in a HIF-1α dependent manner [15]. Inhibition of HIF-1α, but not HIF-2α, was associated with reduced viral replication. Given the multiple roles of HIFs in both the epithelial and immune compartments, we

investigated their involvement in RSV lung disease and pathology by utilizing established inhibitors of HIF-1α (PX478) and HIF-2α (PT2385) in a BALB/c mouse model. Our results underscore the distinct functionality of the individual HIF-α subunits in the development of RSV pathogenesis and indicate the importance of testing HIF therapeutics approved for conditions such as cancer in complex viral respiratory infection biological models for potential benefits, but also unwanted side effects.

3 Materials and methods

3.1 Animal experiments

Female, 8 to 10-week-old BALB/c mice were purchased from Envigo (Indianapolis, IN, USA). Mice received either PX478 or PT2385 by oral gavage at a dose of 20 or 50 mg/kg, respectively. PX478 was dissolved in PBS, while PT2385 was dissolved in 10% DMSO + 90% Corn Oil (CO). For anti-HIF1α, PX478 treated mice were separated into three groups. The first received PBS as the control group. The second received PX478 every 24 h for 10 days (PXQD). The third group received PX478 every 48 h for 10 days (PXQAD). For anti-HIF2α, mice received either CO or PT2385 every 24 h for 10 days. Within 15 minutes of the first treatment, mice were anesthetized and intranasally (IN) inoculated with 50μL of either PBS or RSV Long Strain at a dose of $5x10^6$ PFU. All mice were monitored over the 10-day infection period for changes in bodyweight loss and illness score. Preparation of RSV Long Strain and scoring of illness were done as previously described [16]. All care and procedures involving mice in this study were completed in accordance with the recommendations in the *Guide for the Care and Use of Laboratory Animals* of the National Institutes of Health and the UTMB institutional guidelines for animal care. The Institutional Animal Care and Use Committee (IACUC) of UTMB approved these animal studies under protocol 9001002.

3.2 Bronchoalveolar lavage and viral replication

The BAL fluid was obtained as previously described [17]. A small aliquot was used to determine the total cell count and cellular differentiation of the BAL by cytospin analysis. The remaining BAL fluid was centrifuged, and the supernatants were collected and stored at -80C for future use. To assess viral replication, the right lung was collected from mice at days 2, 4, 7, and 10. Viral replication was evaluated by plaque assay as previously described [17].

3.3 Flow cytometry

At days 4 and 7 p.i., mice were euthanized and the whole lung was collected. The tissue was minced and digested with 10mg/mL DNase I (Sigma-Aldrich, St. Louis, MO, USA) and 50mg/mL collagenase IV (Worthington Biochemical, Lakewood, NJ, USA). The tissue was incubated at 37C for 30 minutes and then passed through a 70-μm cell strainer in RPMI 1640 medium + 10% FBS (CRPMI) and red blood cells were removed by using Red Blood Cell Lysis Buffer (Sigma-Aldrich, Burlington, MA, USA). TruStain FcX (Biolegend, San Diego, CA, USA) was first used to reduce non-specific binding, followed by Zombie NIR Viability dye. To assess CD4+ and CD8+ T-cell populations, the following fluorochrome-labeled antibodies were used: FITC-anti-CD45 (clone 30-F11), BV785-anti-CD3 (clone 17A2), AF 700-anti-CD4 (clone GK1.5), BV510-anti-CD8a (clone 53-6.7), PerCP/Cy5.5-anti-CD44 (clone IM7), BV605-anti-CD62L (clone MEL-14), and PE/Cy7-anti-CD69 (clone H1.2F3). Following surface antibody staining, cells were subjected to fixation and permeabilization overnight using the Foxp3/Transcription Factor Staining Buffer Set (Thermo Fisher Scientific, San Diego, CA, USA). The following day, BV421-anti-Foxp3 (clone MF-14) was added to assess Treg cell populations. All antibodies were purchased from Biolegend or Thermo Fisher Scientific and titrated prior to use. Data were acquired on a BD FACSymphony A5 SE in the UTMB Flow Cytometry Core and analyzed using FlowJo software version 10.9.0 (BD Bioscience, Franklin Lakes, NJ, USA).

3.4 Assessment of airway function and lung histopathology

Bronchoconstriction was evaluated by measuring Penh values in unrestrained mice using whole-body barometric plethysmography (Buxco, Troy, NY, USA) as previously described [18]. Total protein was measured using BioRad Total Protein Dye (Bio-Rad Laboratories, Hercules, CA, USA). LDH activity was measured using the Lactate Dehydrogenase Activity Assay Kit (Sigma-Aldrich, St. Louis, MO, USA). For histology, the left lung was collected from mice at days 4, 7, and 10. The tissue was fixed in 10% neutral buffered formalin and subjected to paraffin embedding. Sections were cut and stained with H&E and evaluated by a board-certified pathologist with expertise in mouse lung (Y.L.J.-H). Assessment of the tissue was done as previously described [19].

3.5 Statistical analysis

Statistical analyses were performed using a two-way mixed ANOVA or an unpaired student's t-test as appropriate. Analyses were done using GraphPad Prism 9.5.1 (GraphPad Software, Inc., San Diego, CA, USA). Results are expressed as mean ± SEM and $p \leq 0.05$ value was selected to indicate significance.

4 Results

4.1 Inhibition of HIF-1α during RSV infection results in worsening clinical disease and schedule dependent regulation of RSV replication.

To start investigating the role of HIF-1α in RSV disease, groups of BALB/c mice were administered PX478 at a dose of 20mg/kg by oral gavage every 24 h (PXQD) over the 10-day infection period (Fig. 1A). Shortly after the first dose of PX478, mice were anesthetized and intranasally (IN) infected with RSV at a dose of $5x10^6$ plaque forming units (PFU). We found mice that received PXQD treatment was associated with worsening body weight and illness score, characterized by an inability to regain weight regardless of infection status (Fig. 1B, 1C). Assessment of viral replication in the lung by plaque assay demonstrated RSV/PXQD mice to have significantly reduced replication at early and peak timepoints of days 2 and 4 p.i., respectively, when compared to the RSV/PBS control mice (Fig. 1D). However, RSV replication in RSV/PXQD mice persisted through day 7 p.i., at levels similar to that of day 4, with some RSV/PXQD mice having detectable replication in the lung tissue as late as day 10 p.i., while RSV/PBS control mice achieved viral clearance by day 7 (Fig. 1D). Together, these data demonstrate the continued suppression of HIF-1α results in worsening clinical disease parameters, even among healthy mice, and is associated with both an anti-viral and pro-viral role in the pathogenesis of RSV.

To improve the effect on body weight loss and illness in the PBS/PXQD mice, the administration of PX478 was changed to every 48 h (PXQAD) over the 10-day infection period (Fig. 1E). Uninfected mice that received PXQAD no longer exhibited substantial weight-loss or heightened illness in comparison to the PBS/PBS mice (Fig. 1F, 1G). Despite this, RSV infected mice treated with PXQAD continued to demonstrate significantly worse body weight-loss and illness score in comparison to the RSV/PBS mice, although showed signs of recovery at the later stages of the disease course. Assessment of viral replication in RSV/PXQAD mice showed reduced RSV replication at days 2 and 4 p.i., with no significant difference in viral clearance at days 7 and 10 p.i. when compared to the RSV/PBS group

(Fig. 1H). Collectively, these data indicate HIF-1α to be important for recovery from RSV infection and to have a complex role in the control of RSV replication.

4.2 Inhibition of HIF-1α leads to reduced immune responses following RSV infection.

The immune response to an RSV infection plays a key role in determining disease severity and the control of RSV replication [20]. To understand the impact of HIF-1α inhibition on the immune response to RSV, we first evaluated the cellular composition of the BAL fluid. Uninfected mice that received PXQD or PXQAD showed no significant modification to the BAL cellular composition as compared to the respective PBS/PBS control groups (Fig. 2A-2H). RSV infected mice that received PXQD demonstrated significant reductions in the number of total cells present in the BAL (Fig. 2A), specifically, in the number of lymphocytes (Fig. 2B) and macrophages (Fig. 2C) at all time points tested. Neutrophil cell counts showed a trend for reduced cell numbers but were not significantly altered as compared to the RSV/PBS control mice (Fig. 2D). RSV infected mice that received PXQAD showed similar patterns in cellular composition, with total cell counts (Fig. 2E), lymphocytes (Fig. 2F), and macrophages (Fig. 2G) being significantly reduced as compared to the RSV/PBS control mice. Neutrophil cell counts were significantly reduced at day 2 p.i. but remained similar to the RSV/PBS control mice at all other time points (Fig. 2H). Together, these data suggest HIF-1α is important for the recruitment of immune cells within the airway space.

$CD4^+$ and $CD8^+$ T-cells are fundamental in controlling RSV replication and clearance within the host [20-22]. With reduced lymphocyte numbers in the BAL and the complex outcome to viral replication, we next wanted to assess the impact of HIF-1α inhibition on the T-cell population within the lung tissue. To do so, flow cytometry analysis was completed using whole lung tissue at days 4 and 7 p.i. as depicted in Fig. S1. Beginning with $CD4^+$ T-cells, RSV infected mice treated with PXQD were found to have significant reductions at day 4 p.i. in $CD4^+$ naïve cells (Fig. 3A), $CD4^+$ effector cells (Fig. 3B), active $CD4^+$ T-cells (Fig. 3C), and $CD4^+$ T-reg cells (Fig. 3D) as compared to the RSV/PBS

control mice. At day 7 p.i., RSV/PXQD mice showed continued significant reductions in $CD4^+$ effector cells and $CD4^+$ T-reg cells. RSV infected mice treated with PXQAD demonstrated significant reductions at day 4 p.i. in $CD4^+$ effector cell and active $CD4^+$ cells (Fig.3B, 3C), with no significant differences in $CD4^+$ naïve cells or $CD4^+$ T-reg cells as compared to the RSV/PBS control mice (Fig.3A, 3D). No significant differences were noted in any $CD4^+$ T-cell type at day 7 p.i. between RSV/PXQAD and the RSV/PBS control mice. Comparative analysis between RSV/PXQD and RSV/PXQAD showed RSV infected mice receiving PX478 treatment every 24 h to have a greater reduction in $CD4^+$ naïve cells, $CD4^+$ effector cells, and $CD4^+$ T-reg cells than those receiving PX478 every 48 h (Fig. 3A, 3B, 3D).

For $CD8^+$ T-cells, RSV/PXQD and RSV/PXQAD mice had significant reductions in $CD8^+$ naïve cells at day 4 p.i. as compared to the RSV/PBS control mice (Fig. 3E). The number of $CD8^+$ effector cells (Fig. 3F) and active $CD8^+$ cells (Fig. 3G) were similar across all groups. At day 7 p.i., the number of $CD8^+$ effector cells and active $CD8^+$ T-cells were significantly reduced for both RSV/PXQD and RSV/PXQAD as compared to the RSV/PBS control mice (Fig. 3F, 3G). Comparative analysis between RSV/PXQD and RSV/PXQAD showed RSV infected mice receiving PX478 treatment every 24 h to have a greater reduction in $CD8^+$ naïve cells, $CD8^+$ effector cells, and active $CD8^+$ cells than those receiving PX478 every 48 h (Fig. 3E-3G). Collectively, these data indicate that HIF-1α plays an essential role in regulating T-cell responses during RSV infection.

4.3 Inhibition of HIF-1α improves airway function and lung inflammation during RSV infection.

HIFs have a fundamental role in lung function and the tissue repair process [23]. To assess airway function during RSV infection, we first measured bronchoconstriction using whole-body plethysmography as previously described [17]. Uninfected mice that received PXQD or PXQAD showed no significant alterations to Penh values at any timepoint tested as compared to the respective

PBS/PBS control groups (Fig. 4A, 4D). RSV infected mice that received PXQD or PXQAD had significant improvements in Penh at days 1, 5, and 6 p.i., with values comparable to the PBS/PBS control mice throughout the disease course (Fig. 4A, 4D). We next measured total protein and LDH activity in the BAL fluid as an indicator of epithelial damage and generalized cell death, respectively. Uninfected mice that received PXQD or PXQAD showed no significant differences in total protein or LDH activity at any timepoint tested as compared to the respective PBS/PBS control mice (Fig. 4C-4F). Interestingly, RSV/PXQD mice had significant improvements in both total protein and LDH activity at day 4 p.i. as compared to the RSV/PBS control mice (Fig. 4B, 4C). There were no significant differences in total protein at days 7 or 10 p.i., though the RSV/PXQD mice did have an increasing trend in LDH activity at these timepoints consistent with the continued replication noted in Fig. 1D. Similarly, RSV/PXQAD mice had significant improvements to total protein at day 4 p.i. as compared to the RSV/PBS control mice (Fig. 4E). RSV/PXQAD mice had no changes to total protein at days 7 and 10 p.i., and no alteration to LDH activity at any timepoint as compared to the RSV/PBS control mice (Fig. 4E, 4F).

We next assessed the lung tissue of mice that received PXQAD by histopathology. Based on the scoring determined by a board-certified veterinarian with expertise in mouse lung morphology, uninfected mice that received PXQAD remained comparable to the PBS/PBS control mice in all categories and at all timepoints tested. RSV/PXQAD mice demonstrated significant improvements to the total lung score as compared to the RSV/PBS control mice (Fig. 5A). Specifically, perivasculitis (Fig. 5B) and peribronchiolitis (Fig. 5C) were significantly improved at days 4 and 7 p.i. as compared to the RSV/PBS control mice. This finding is consistent with the reduction of immune cells noted in the BAL and lung tissue of these mice (Fig. 2,3). No significant differences in the percent of abnormal lung field (Fig. 5D) or the severity of interstitial pneumonia (Fig. 5E) were appreciated at any time point. Representative images of the lung tissue for RSV/PBS and RSV/PXQAD mice are shown in

Fig.5F. Collectively, these data suggest HIF-1α to contribute to the worsening of airway function and tissue damage during the acute phase of RSV infection.

4.4 Inhibition of HIF-2α results in improved clinical disease and antiviral activity during RSV infection.

While there exists a degree of functional overlap between the HIF-α subunits, they have also been demonstrated to govern a distinct range of biological activities. To better understand the specific role of HIF-2α during RSV infection, mice were administered PT2385 in DMSO+Corn-oil (CO) by oral gavage every 24 h at a dose of 50mg/kg (Fig. 6A). Shortly after the first dose, mice were anesthetized and infected with RSV at a dose of $5x10^6$ PFU. Uninfected mice that received PT2385 were found to have similar body weight loss and illness score as the PBS/CO control mice (Fig. 6B-6C). RSV infected mice that received PT2385 demonstrated significant improvements to bodyweight loss at nearly all timepoints over the 10-day disease course as compared to the RSV/CO control mice (Fig. 6B). Interestingly, the illness score in RSV/PT2385 mice was worse at day 4 p.i. but showed a quicker recovery at later time points of infection when compared to the RSV/CO control mice (Fig. 6C). Assessment of viral replication in the lung tissue by plaque assay showed RSV/PT2385 mice to have reduced RSV replication at early and peak timepoints of days 2 and 4 p.i. (Fig. 6D). By days 7 and 10 p.i., no replicating virus was detected in RSV/PT2385 mice, indicating successful clearance of RSV from the lung tissue. Collectively, these data suggest HIF-2α to contribute to RSV-induced disease and the promotion of viral replication.

4.5 Inhibition of HIF-2α leads to increased immune activity in the BAL and lung tissue of RSV infected mice.

We previously demonstrated HIF-2α to be dispensable for the control of RSV replication in small airway epithelial cell [15]. Given the antiviral outcome in RSV/PT2385 mice, we next wanted to understand the contribution of HIF-2α to the immune response during an RSV infection. We first evaluated the cellular composition of the BAL fluid. Uninfected mice that received PT2385 showed

no significant difference in BAL cellular composition as compared to the PBS/CO control groups (Fig. 7A-7D). RSV infected mice that received PT2385 demonstrated a significant increase in the number of total of cells present in the BAL (Fig. 7A), specifically, in the number of lymphocytes (Fig. 7B). Macrophage cell counts (Fig. 7C) were significantly increased only at days 2 and 10 p.i., while neutrophil cell counts (Fig. 7D) remained comparable to the RSV/CO control mice.

As with HIF-1α, we next assessed $CD4^+$ and $CD8^+$ T-cell responses using flow cytometry analysis. Starting with $CD4^+$ T-cells, we observed an increasing trend at day 4 p.i. in $CD4^+$ naïve cells (Fig. 8A) as well as significant increases in $CD4^+$ effector cells (Fig. 8B) and active $CD4^+$ T-cells (Fig. 8C)) in RSV/PT2385 mice as compared to the RSV/CO control mice. By day 7 p.i., all $CD4^+$ T-cells in the RSV/PT2385 were of comparable number to the RSV/CO control mice. Additionally, no changes in $CD4^+$ Treg cells were noted at days 4 or 7 p.i. in RSV/PT2385 mice as compared to the RSV/CO control mice (Fig. 8D). For $CD8^+$ T-cells, we observed significant increases at day 4 p.i. in $CD8^+$ naïve cells (Fig. 8E), $CD8^+$ effector cells (Fig. 8F), and active $CD8^+$ cells (Fig. 8G). On day 7 p.i., the number of active $CD8^+$ T-cells (Fig. 8G) remained significantly increased, while $CD8^+$ naïve and effector cell numbers were comparable to the RSV/CO control mice. Collectively, these data show the inhibition of HIF-2α results in increased T-cell numbers, likely contributing to an earlier control of RSV replication. This suggests HIF-2α functions to suppress T-cell responses during RSV infection.

4.6 Inhibition of HIF-2α does not modify airway function during RSV infection.

To assess airway function during RSV infection, we first measured bronchoconstriction. Uninfected mice that received PT2385 showed no significant alterations to Penh values at any timepoint tested as compared to the PBS/CO control mice (Fig. 9A). Similarly, RSV infected mice treated with PT2385 had similar Penh values as the RSV/CO control mice throughout the 10-day disease course. We next measured total protein and LDH activity in the BAL. We observed no significant differences in total protein for all mice tested as compared to their respective control groups

(Fig. 9B). Interestingly, RSV/PT2385 mice had significantly elevated LDH activity at days 2 and 4 p.i. (Fig. 9C), consistent with the moderate increase in immune cell numbers (Fig. 7, Fig. 8). By day 7 p.i., LDH activity was comparable to the RSV/CO control mice. No significant differences in LDH activity were appreciated between PBS/PT2385 and the PBS/CO control mice at any timepoint tested.

Lastly, we assessed the lung tissue of mice that received PT2385 by histopathology. Based on the scoring determined by a board-certified veterinarian with expertise in mouse lung morphology, uninfected mice that received PT2385 remained comparable to the PBS/CO control mice in all categories and at all time points tested. RSV infected mice treated with PT2385 demonstrated significant improvements at day 10 p.i. to the total lung score (Fig. 10A), in peribronchiolitis (Fig. 10B), and to the severity of interstitial pneumonia (Fig. 10C) as compared to the RSV/CO control mice. The percent abnormal lung field (Fig. 10D) was found to have a trend towards improvement in RSV/PT2385 mice and perivasculitis (Fig. 10D) was significantly worse as compared to the RSV/CO control mice. Representative images of the lung tissue for RSV/CO and RSV/PT2385 mice are shown in Fig.10F. Collectively, these data suggest HIF-2α does not modify airway function, but does contribute to worsening lung pathology during the acute phase of RSV infection.

5 Discussion

The pharmacological use of HIF therapeutics has been extensively explored in various models of cancer, autoimmunity, and non-infectious lung damage [8, 24, 25]. While some studies have demonstrated the antiviral potential of HIF inhibitors against respiratory viruses, these findings have been primarily limited to *in vitro* characterizations [9]. To date, there are no reports investigating the therapeutic potential of a HIF inhibitor against a viral respiratory infection in a relevant animal model. Our laboratory has previously shown that RSV infection results in the stabilization of both HIF-1α and HIF-2α. Through pharmacological inhibition of HIF, we also demonstrate the stabilization of HIF-1α, but not HIF-2α, to orchestrate metabolic reprogramming towards glycolysis and for this activity to be

important for RSV replication in lung epithelial cells [15]. Given the diverse biological role of HIFs across several cellular compartments, we next wanted to understand the function of these inhibitors in a BALB/c mouse model of RSV infection. In the present study, we find the inhibition of HIF-1α by PX478 to worsen clinical disease while concurrently improving aspects of airway function during RSV infection. HIF-1α inhibition also resulted in initial antiviral activity followed by a loss of viral clearance at later time points of infection when PX478 was given daily, but not every-other-day. We show this variation in viral clearance to likely be driven by a schedule-dependent reduction in $CD4^+$ and $CD8^+$ T-cells. In contrast, inhibition of HIF-2α by PT2385 was found to improve clinical disease with no difference to airway function. Inhibition of HIF-2α also resulted in antiviral activity following RSV infection with no impact on viral clearance. This antiviral activity is likely due to a heightened immune response, characterized by an increase in $CD4^+$ and $CD8^+$ T-cell activity. Taken together, these data emphasize a unique and complex role for HIFs in the context of RSV infection.

During our initial experiments with PX478, we observed notable weight loss and increased illness in the PBS/PXQD mice compared to the PBS control mice. However, when analyzing various factors such as BAL cells, airway function, total protein, and LDH activity we found no significant differences between the two groups. This suggests that the deteriorating clinical condition in PBS/PXQD mice is likely influenced by a factor other than inflammation or tissue damage. It's worth noting that, apart from the time interval, we are administering a dose similar to or less than what is reported in the literature [26-28]. Studies investigating the anti-tumor efficacy of PX478 have administered this compound for up to 5 consecutive days, reporting minor weight-loss in the mice during this time [28, 29]. Based on our review, we believe we are the first to administer PX478 for longer than 5 consecutive days. Other cancer models have delivered PX478 every ~2-3 days for extended periods and report no negative effects in mice [30, 31]. Moreover, PX478 has been well-tolerated by patients in a phase-1 clinical trial with the most common side effect reported to be nausea

[32, 33]. Interestingly, studies using obese mouse models have noted PX478 to prevent weight gain [34, 35]. Additionally, a recent investigation has shown the efficacy of PX478 as a potential therapeutic for type-II diabetes [36]. Considering the significant role of HIF-1α in metabolic function and the recent repositioning of PX478 for treatment of type-II diabetes, it is possible that consecutive dosing of PX478 for extended periods of time may lead to appetite suppression. In our model, spacing treatments over 48 h ameliorated this effect, resulting in patterns of clinical disease in the PBS/PXQAD mice that resemble previously reported observations. Despite this, RSV infected mice treated with PX478 every 48 h continued to display delayed recovery as compared to the RSV control mice (Fig. 1F). This was surprising as these RSV infected mice effectively cleared the virus from the lung tissue and show no signs of increased inflammatory activity. One possible explanation for the phenomenon could be a moderate appetite suppression induced by PX478 that is amplified due to the stress of infection.

In RSV-infected mice, inhibition of both HIF-1α or HIF-2α showed antiviral activity. However, based on our previous characterizations in epithelial cells and the cellular responses noted in this study, the mechanisms underlying this activity appear to be distinct for each HIF-α subunit [15]. Treatment with PX478 during RSV infection resulted in a suppressed immune response, suggesting that the antiviral activity is more likely attributed to partially impaired RSV replication rather than immune-mediated clearance. A primary role of HIF-1α is to regulate metabolic activity within the cell [37]. Our laboratory and others have previously shown RSV infection to alter host cell metabolism, favoring glycolysis, and for this to be important for RSV replication [15, 38, 39]. Inhibition of HIF-1α in RSV infected mice may reduce the glycolytic capacity within lung epithelial cells, effecting replication. Additionally, RSV infection has been shown to induce autophagy and the inhibition of this process has a profound impact on RSV replication [40-42]. HIF-1α is instrumental in the autophagic pathway, inducing the expression of pro-autophagic genes like BNIP3 and BNIP3L/NIX, directly

upregulating autophagy-related genes (ATG) such as ATG5, ATG7, and ATG12, and promoting proteins crucial for autophagosome formation [43, 44]. In addition to shifts in metabolism, it is likely that the autophagy pathway is also disrupted due to HIF-1α inhibition, further contributing to reduced RSV replication.

Despite this antiviral activity, RSV-infected mice treated with PXQD continued to exhibit prolonged viral replication on days 7 and 10 p.i., in contrast to RSV/PXQAD mice and RSV/PBS control mice, which had effectively cleared RSV from the lung tissue at those time points. HIF-1α is critical for the activation, migration, and cytotoxic functions of T-cells [45]. T-cells play an important role in controlling RSV replication and clearance within the host [20-22]. During the early stages of RSV disease, $CD4^+$ effector cells are known to aid in the recruitment and activation of other immune cells that control RSV replication such as natural killer (NK) cells, $CD8^+$ cytotoxic T-cells, and B-cells [46-48]. At day 4 p.i., or peak replication, $CD4^+$ T-cell number and activation were found to be reduced in all RSV/PX478 treated mice (Fig. 3). This would suggest HIF-1α-mediated $CD4^+$ T-cell responses to be dispensable for the direct control of RSV replication at early timepoints, but may still impact the recruitment of $CD8^+$ T-cells at later timepoints. At later stages of disease, $CD8^+$ effector T-cells are responsible for directly clearing RSV from the lung epithelium [49]. RSV/PXQD mice were found to have a greater suppression of effector $CD8^+$ T-cells and active $CD8^+$ T-cells when compared to RSV/PXQAD mice. Based on this, it is likely that RSV/PXQAD mice retained a $CD8^+$ T-cell threshold sufficient to clear the virus from the lung tissue, explaining the differences in viral clearance between the two treatment regimens.

Like PX478, treatment with PT2385 demonstrated significant antiviral activity at early and peak timepoints of RSV replication. RSV/PT2385 mice displayed a moderate increase in immune cell presence, characterized by heightened $CD4^+$ and $CD8^+$ T-cell number and activity. Since HIF-2α was

shown to be dispensable for RSV replication in epithelial cells, it is probable that this increase in T-cell activity could explain the observed antiviral effects seen in RSV/PT2385 mice. Although, HIF-2α is known to have important roles in regulating immune responses, its specific contribution to T-cell function is not as extensively studied as HIF-1α [45]. Recently, a loss of HIF-2α in regulatory T-cells (Treg) was described to reduce Treg suppressor functions, leading to an increase in $CD4^+$ T-cell activity, without altering Treg development [50, 51]. In agreement with this finding, our results indicate an increase in $CD4^+$ and $CD8^+$ T-cell activity with no significant alteration to Treg cell numbers as compared to the RSV/PBS control mice. Furthermore, treatment of Tregs and $CD4^+$ T-cells with PT2385 was found to result in an increase in HIF-1α expression [51]. As previously mentioned, HIF-1α is a potent inducer of T-cell activation and migration. Therefore, it is possible for these $CD4^+$ and $CD8^+$ T-cells to have enhanced numbers and activity due to failed suppression by Treg cells and to an increase in HIF-1α, leading to the observed antiviral activity and earlier recovery from RSV disease in RSV/PT2385 mice.

HIF-1α has been demonstrated to impact airway function in a variety of ways, including the induction of bronchoconstriction [52]. HIF-1α achieves this by influencing the contractility of airway smooth muscles through several mechanisms such as stimulating calcium production, modulating ion channels, and triggering the release of mediators like leukotrienes [53-55]. In contrast, HIF-2α has been shown to be dispensable for the induction of changes to airway hypersensitivity and bronchoconstriction [50]. Consistent with these findings, we observed notable improvements in bronchoconstriction in RSV-infected mice treated with PX478 but not with PT2385. In the PXQAD experiments, pathology scores for perivasculitis and peribronchiolitis were significantly improved on days 4 and 7 p.i., as compared to the RSV control mice. This finding is consistent with the reduced immune cell infiltration and antiviral activity at these timepoints. By day 10 p.i., the lung tissue of RSV/PXQAD was comparable to the RSV/PBS control mice. As HIF-1α has important roles at the

later stages of lung injury in promoting angiogenesis and tissue regeneration [56], it is possible that inhibition of HIF-1α at the later stages of disease may hinder proper tissue repair, negating the benefit observed in the initial phase of RSV lung disease. Mice treated with PT2385 during RSV infection had no major alterations to any scored category until day 10 p.i., consistent with the lack of improvement in airway function in these mice. By the end of the acute phase, RSV/PT2385 mice had moderate increases in perivasculitis, but significant improvements in all other categories. This increase in perivasculitis could be due to the increase in the number of immune cells observed within the BAL and lung tissue. Additionally, it could also be related to changes in vascular function, as HIF-2α plays an important role in maintaining the vascular integrity [57].

Collectively, our data demonstrate HIF-1α and HIF-2α to be potent regulators of the immune response to RSV infection. We also highlight HIF-1α as a critical component to the onset of RSV-induced bronchoconstriction. Additionally, these data describe the novel and complex contribution of the HIF-α subunits to RSV replication and clearance. Though we show antiviral potential for both HIF-α inhibitors, the resulting impact to clinical disease and modulation of the immune response warrant great care be taken when considering HIF-α inhibitors for therapeutic use against a viral respiratory infection. Furthermore, as our data demonstrates the continued inhibition of HIF-1α to result in prolonged viral replication, our study also highlights the possible unwanted side effects associated with the use of HIF modulating therapeutics in the context of other diseases, such as cancer. Future investigations will focus on further understanding the underlying mechanistic contribution of HIFs to the immune response and tissue repair processes during RSV infection.

6 Conflict of Interest

The authors declare that the research was conducted in the absence of any commercial or financial relationships that could be construed as a potential conflict of interest.

7 Author Contributions

Performed experiments, D.R.M., Y.Q., T.I., and T.L; performed histopathology analysis, Y.L.J.H; contributed to data analysis and drafting of the manuscript, D.R.M.; contributed to the conception of the manuscript, literature review, and final manuscript editing, D.R.M., A.C. and R.P.G. All authors have read and agreed to the published version of the manuscript.

8 Funding

DRM was supported by the McLaughlin Endowment Predoctoral Fellowship and the NIH Clinical and Translational Science Award NRSA (TL1) Training Core TL1TR001440. This research was additionally funded by an Institute for Human Infections and Immunity (IHII) Pilot Grant and by NIH grants AI62884 and AI175955.

9 Acknowledgments

We would like to thank Vineet Menachery, Yuejin Liang, Casey Wright, and Xiaoyi Yuan for their thoughtful discussion. We would also like to thank the Texas A&M University Veterinary Medicine and Biomedical Sciences Research Histology Core Facility for their assistance with the tissue processing. Biorender.com was used to produce the experimental design summaries.

10 Supplementary Material

Figure S1. Schematic for analysis of $CD4^+$ and $CD8^+$ T-cells by flow cytometry.

11 Figures

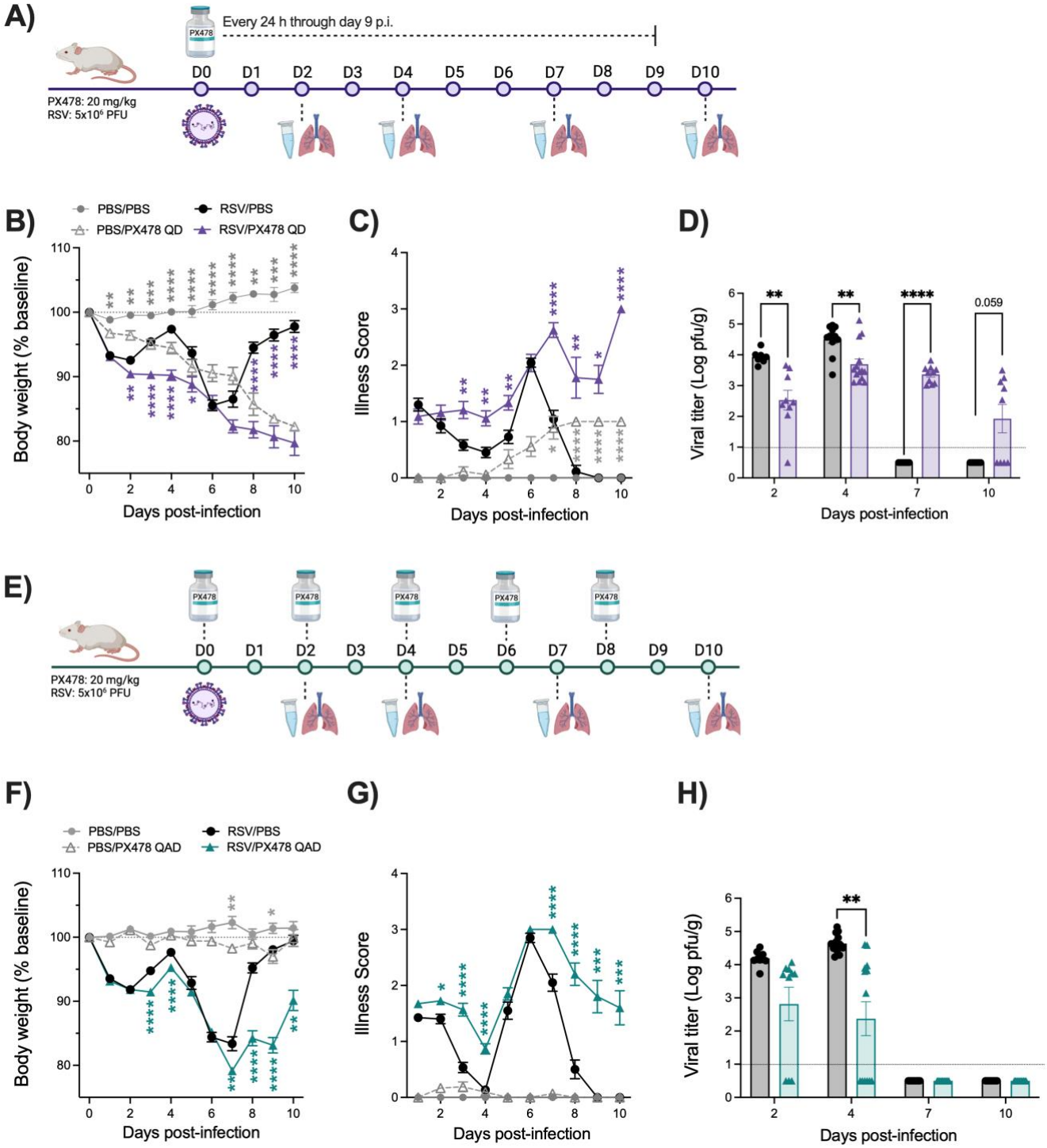
A)
Every 24 h through day 9 p.i.
PX478
D0 D1 D2 D3 D4 D5 D6 D7 D8 D9 D10
PX478: 20 mg/kg
RSV: 5x10⁶ PFU
B)
PBS/PBS
RSV/PBS
PBS/PX478 QD
RSV/PX478 QD
Body weight (% baseline)
Days post-infection
C)
Illness Score
Days post-infection
D)
Viral titer (Log pfu/g)
0.059
Days post-infection
E)
PX478
D0 D1 D2 D3 D4 D5 D6 D7 D8 D9 D10
PX478: 20 mg/kg
RSV: 5x10⁶ PFU
F)
PBS/PBS
RSV/PBS
PBS/PX478 QAD
RSV/PX478 QAD
Body weight (% baseline)
Days post-infection
G)
Illness Score
Days post-infection
H)
Viral titer (Log pfu/g)
Days post-infection

<u>Figure 1.</u> *Assessment of clinical disease and viral replication following HIF-1α inhibition during RSV infection.* The outcomes for mice treated with PX478 QD are shown in (A-D) and for mice treated with PX478 QAD are shown in (E-H). Experimental designs for PXQD and PXQAD are described in (A, E). Following treatment, all mice were monitored daily for changes in (B, F) bodyweight loss and (C, G) illness score. At days 2, 4, 7, and 10 p.i., the right lung was collected for assessment of (D, H) viral replication by plaque assay. For clinical disease, data are pooled from four independent experiments ($n \leq 75$ mice/group). For viral replication, data are pooled from two independent experiments ($n \leq 14$ mice/group). Data are expressed as mean ± SEM. Significant results were determined by two-way mixed ANOVA (* $p \leq 0.05$, ** $p \leq 0.01$, *** $p \leq 0.001$, **** $p \leq 0.0001$).

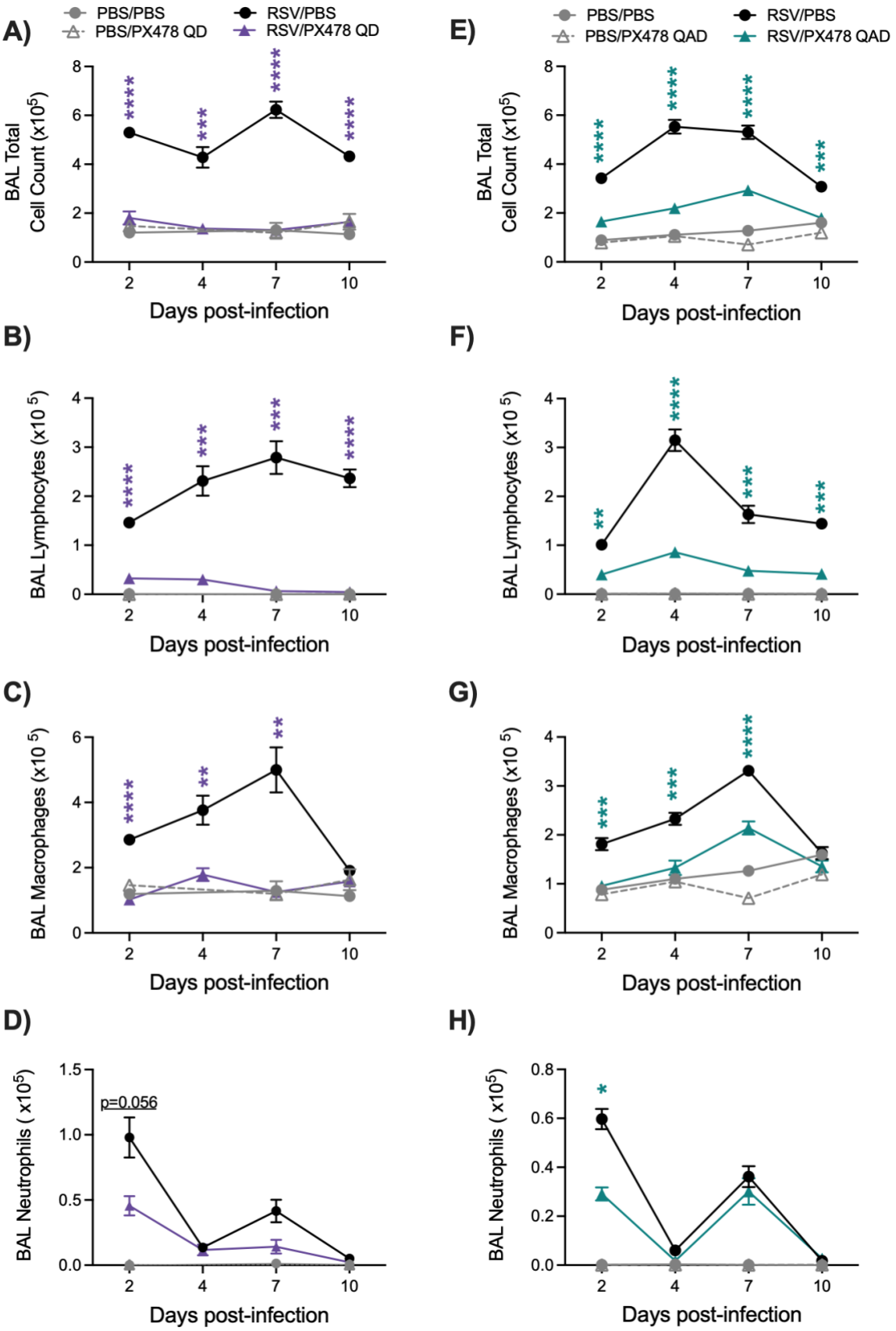
A)
PBS/PBS
PBS/PX478 QD
RSV/PBS
RSV/PX478 QD
BAL Total Cell Count (x10^5)
Days post-infection
E)
PBS/PBS
PBS/PX478 QAD
RSV/PBS
RSV/PX478 QAD
BAL Total Cell Count (x10^5)
Days post-infection
B)
BAL Lymphocytes (x10 5)
Days post-infection
F)
BAL Lymphocytes (x10 5)
Days post-infection
C)
BAL Macrophages (x10 5)
Days post-infection
G)
BAL Macrophages (x10 5)
Days post-infection
D)
p=0.056
BAL Neutrophils (x10^5)
Days post-infection
H)
BAL Neutrophils (x10^5)
Days post-infection

<u>Figure 2.</u> *Differential cell count of the BAL fluid following HIF-1α inhibition during RSV infection.* At days 2, 4, 7, or 10 p.i., BAL fluid was collected from mice that had received (A-D) PXQD or (E-H) PXQAD over the 10-day infection period. This BAL was used to obtain (A, E) total cell counts, as well as differential cell counts consisting of (B, F) lymphocytes, (C, G) macrophages, and (D, H) neutrophils. Data are pooled from two independent experiments ($n \leq 15$ mice/group). Data are expressed as mean ± SEM. Significant results were determined by two-way mixed ANOVA (* $p \leq 0.05$, ** $p \leq 0.01$, *** $p \leq 0.001$, **** $p \leq 0.0001$).

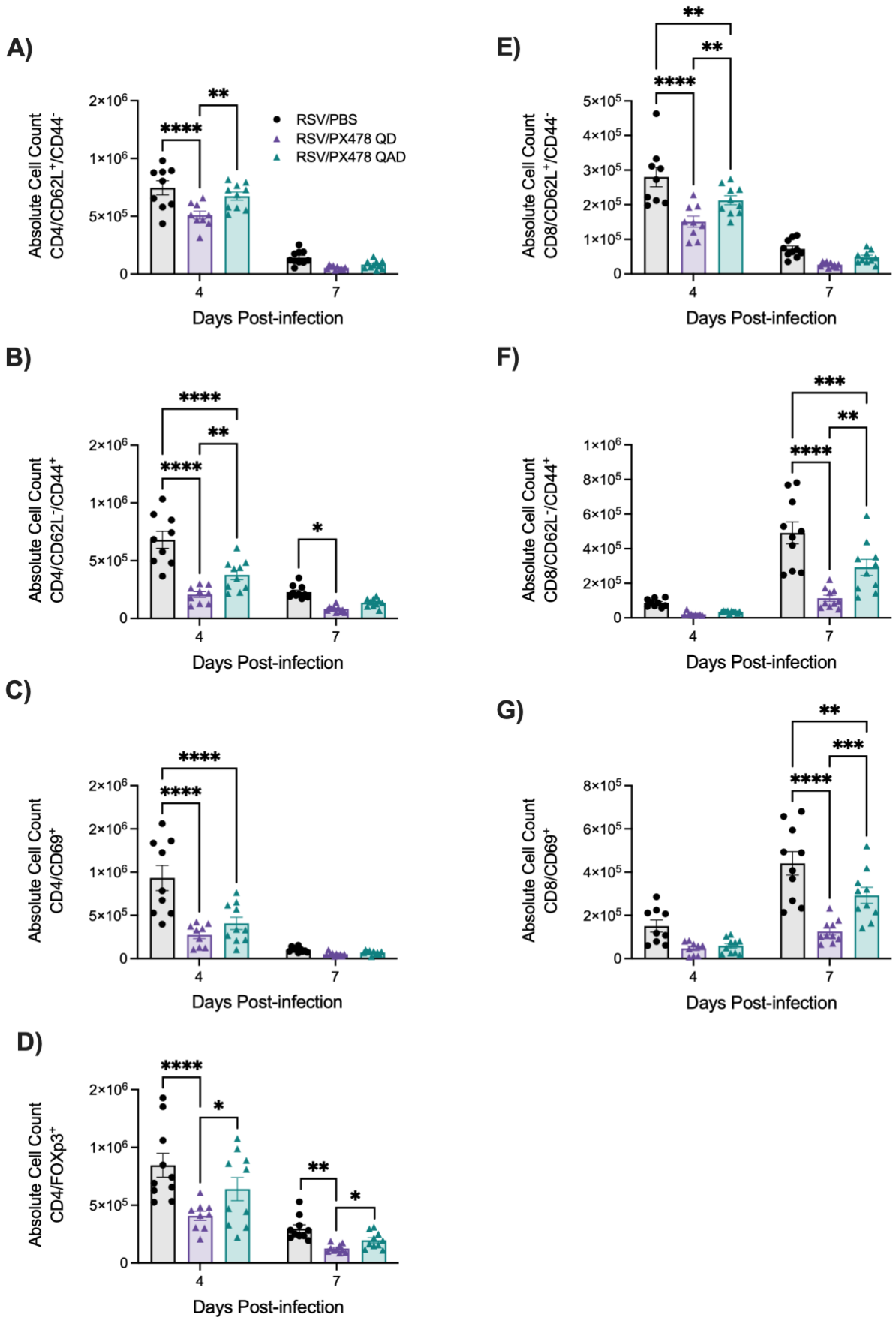
A)
Absolute Cell Count CD4/CD62L+/CD44-
RSV/PBS
RSV/PX478 QD
RSV/PX478 QAD
Days Post-infection
B)
Absolute Cell Count CD4/CD62L-/CD44+
Days Post-infection
C)
Absolute Cell Count CD4/CD69+
Days Post-infection
D)
Absolute Cell Count CD4/FOXp3+
Days Post-infection
E)
Absolute Cell Count CD8/CD62L+/CD44-
Days Post-infection
F)
Absolute Cell Count CD8/CD62L-/CD44+
Days Post-infection
G)
Absolute Cell Count CD8/CD69+
Days Post-infection

<u>Figure 3.</u> *Assessment of CD4$^+$ and CD8$^+$ T-cells following HIF-1α inhibition during RSV infection.* Whole lung tissue was collected at peak RSV replication and a timepoint of viral clearance, days 4 and 7 p.i., respectively. Single cell suspension was prepared, stained with live/dead cell dye and fluorochrome-conjugated antibodies, and acquired by flow cytometry. Data were analyzed for (A) CD4$^+$ naive cells, (B) CD4$^+$ effector cells, (C) active CD4$^+$ cells, (D) CD4$^+$ Treg cells, (E) CD8$^+$ naive cells, (F) CD8$^+$ effector cells, and (G) active CD8$^+$ cells. Black circle = RSV/PBS, purple triangle = RSV/PXQD, and green triangle = RSV/PXQD. Data are pooled from two independent experiments (n $\leq$ 10 mice/group). Data are expressed as mean ± SEM. Significant results were determined by two-way mixed ANOVA (* $p \leq 0.05$, ** $p \leq 0.01$, *** $p \leq 0.001$, **** $p \leq 0.0001$).

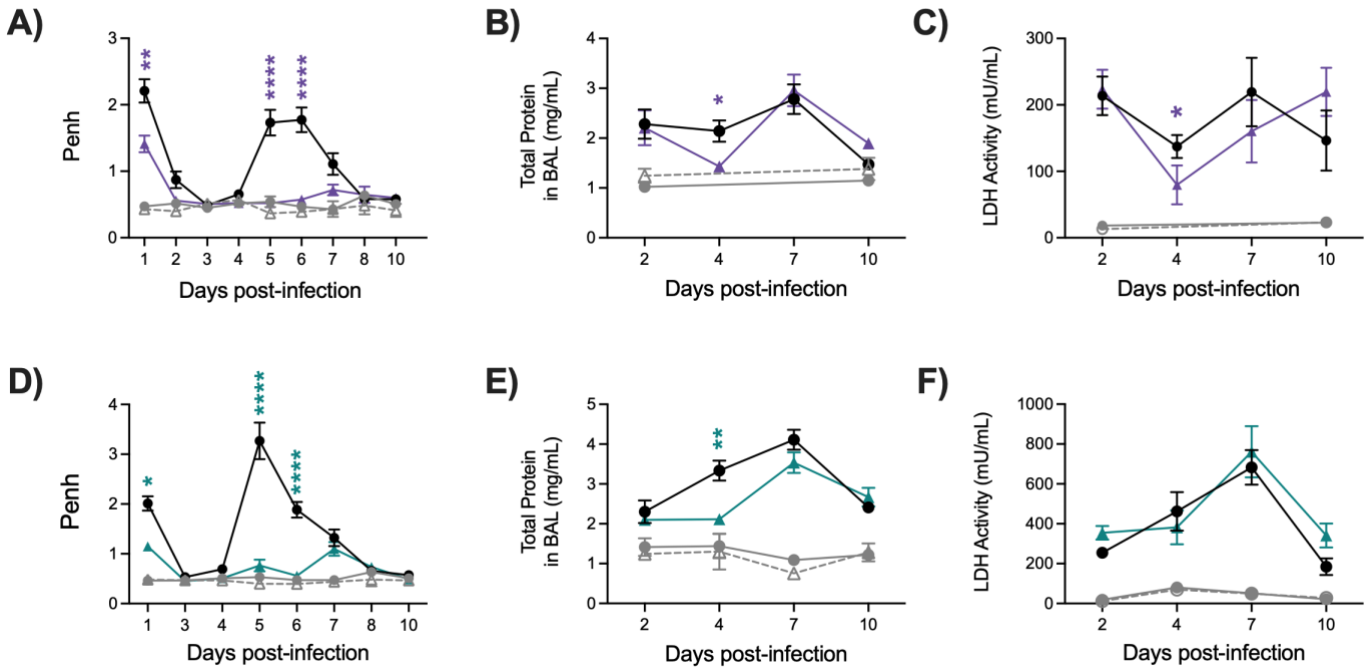

Figure 4. *Assessment of airway function following HIF-1α inhibition during RSV infection.* Airway function was determined in mice that received PXQD (A-C) or PXQAD (D-F) over the 10-day infection period. (A, D) Bronchoconstriction, represented by baseline Penh, was measured by plethysmography. Using BAL fluid collected at days 2, 4, 7, or 10 p.i., (B, E) total protein and (C, F) LDH were measured. For bronchoconstriction, data are pooled from three independent experiments (n ≤ 60 mice/group). For total protein and LDH, data are pooled from two independent experiments (n ≤ 10 mice/group). Data are expressed as mean ± SEM. Significant results were determined by two-way mixed ANOVA (* $p \leq 0.05$, ** $p \leq 0.01$, **** $p \leq 0.0001$).

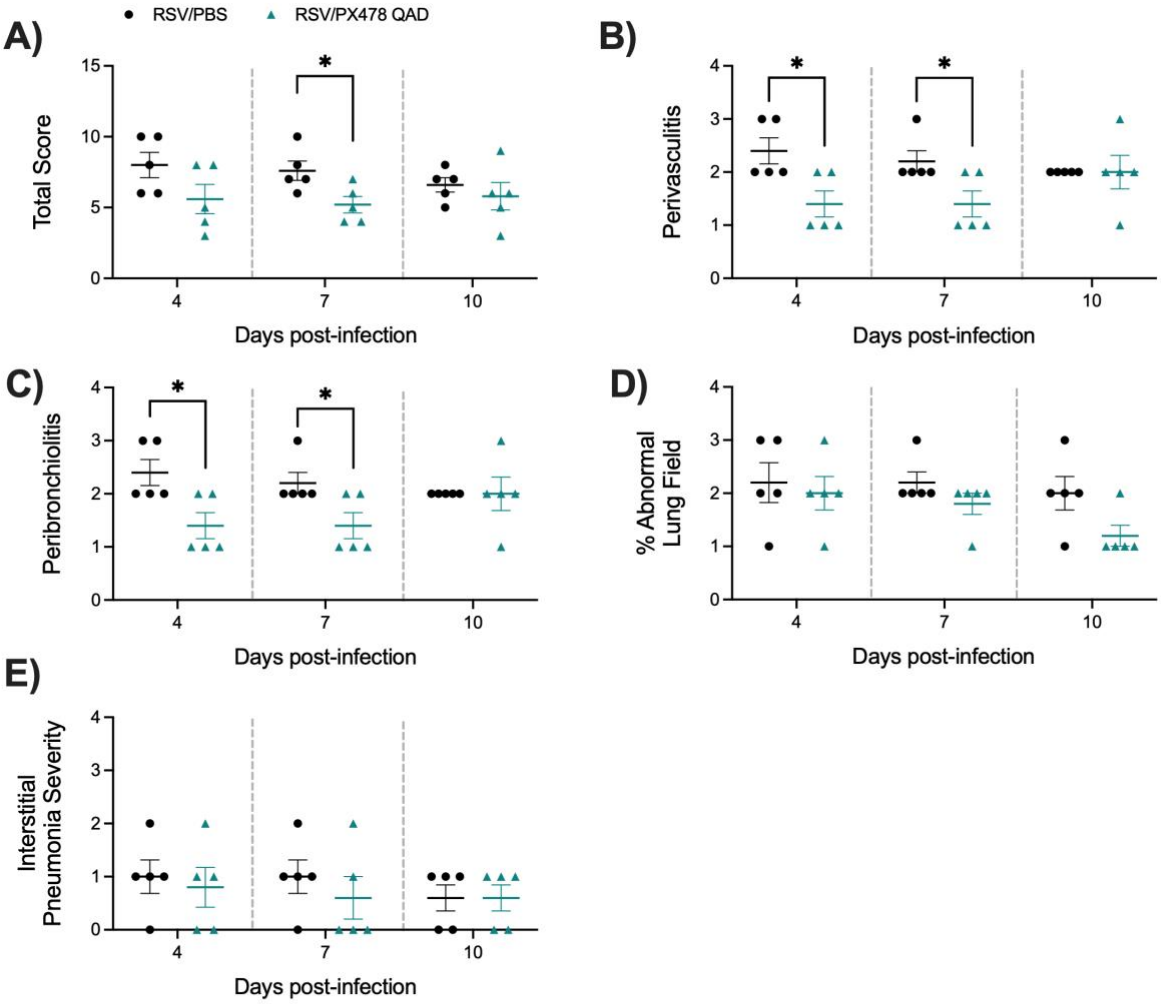
A)
RSV/PBS
RSV/PX478 QAD
Total Score
Days post-infection
B)
Perivasculitis
Days post-infection
C)
Peribronchiolitis
Days post-infection
D)
% Abnormal Lung Field
Days post-infection
E)
Interstitial Pneumonia Severity
Days post-infection

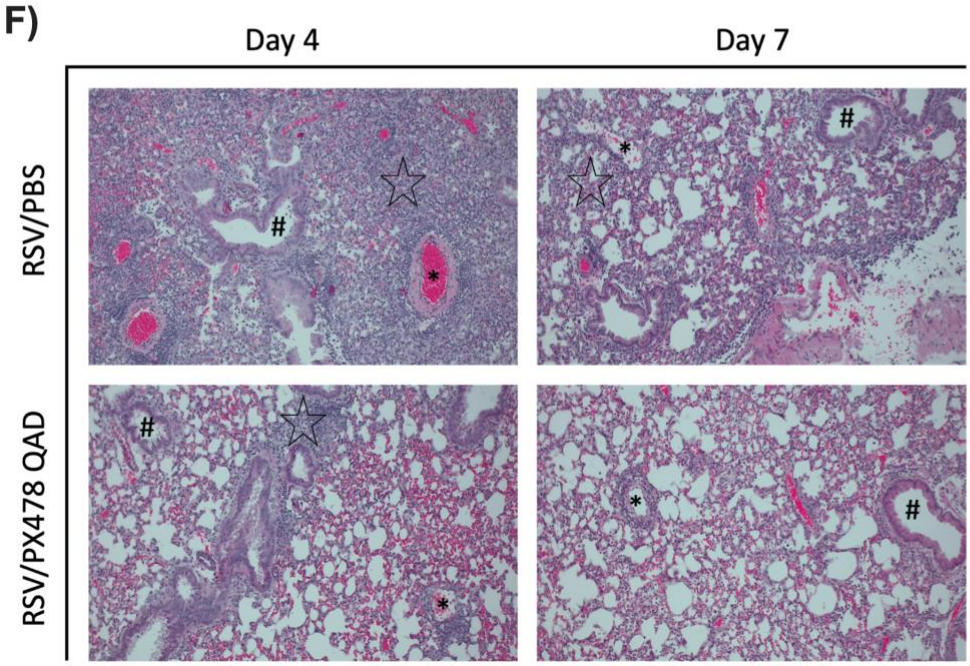
F)
Day 4
Day 7
RSV/PBS
RSV/PX478 QAD

Figure 5. *Histopathological scoring of lung tissue following HIF-1α inhibition during RSV infection.* At days 4, 7, and 10 p.i., the left lung was collected from RSV infected mice that had received PBS or PXQAD and subjected to FFPE. Cuts of lung tissue were stained with H&E and observed under a microscope at 10X magnification. The (A) total score was calculated, consisting of scores for (B) perivasculitis, (C) peribronchiolitis, (D) percent abnormal lung field, and (E) interstitial pneumonia. Representative images are shown in (F). Perivasculitis is indicated by an asterisk. Peribronchiolitis is indicated by the hash sign. Interstitial pneumonia is indicated by the black star. No interstitial pneumonia present in RSV/PX478 QAD on day 7. Data are representative of one independent experiment (n = 5 mice/group). Data are expressed as mean ± SEM. Significant results were determined by an unpaired student's t-test (* $p \leq 0.05$).

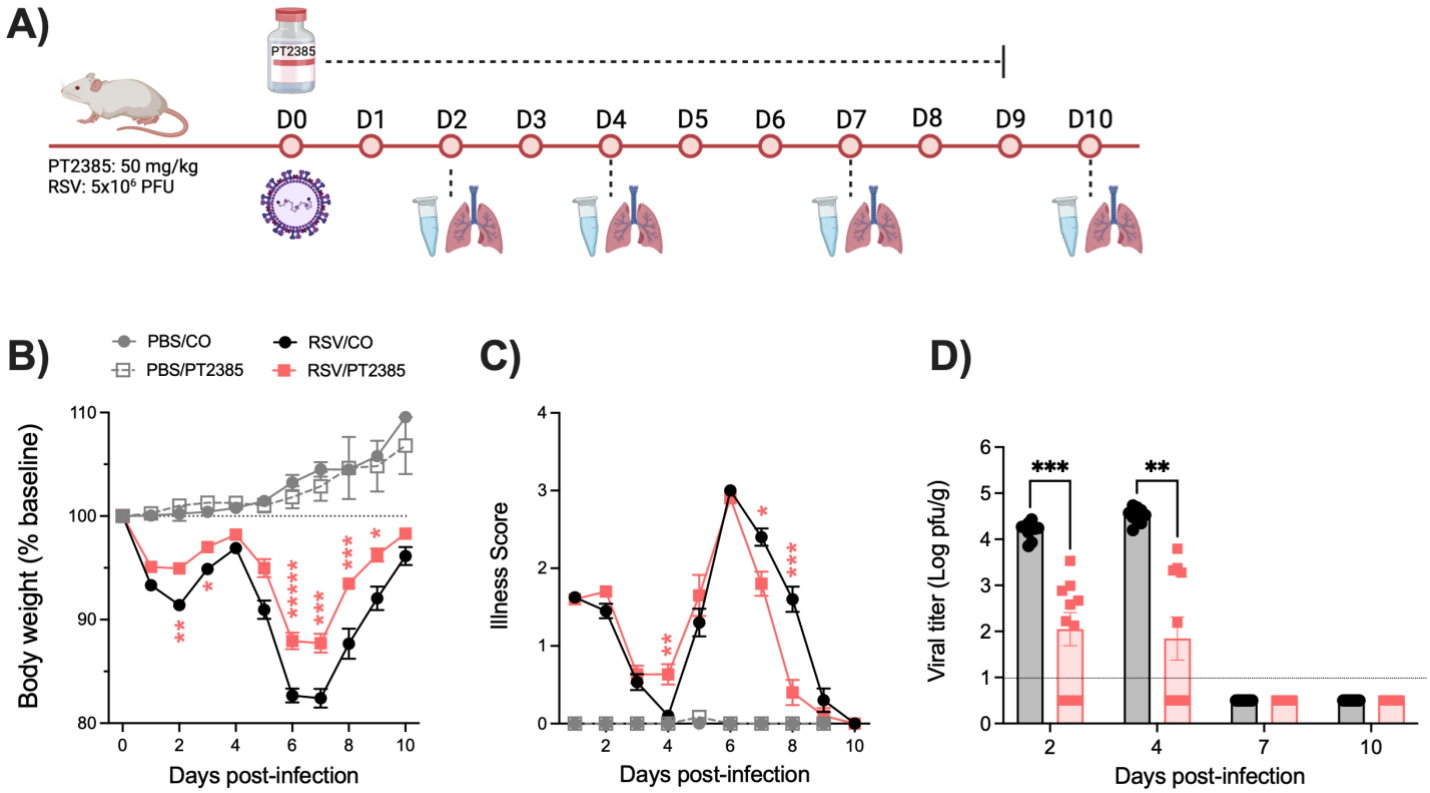

483 **Figure 6.** *Assessment of clinical disease and viral replication following HIF-2α inhibition during RSV*
484 *infection.* The experimental design for mice treated with PT2385 is described in (A). Following
485 treatment, all mice were monitored daily for changes in (B) bodyweight loss and (C) illness score. At
486 days 2, 4, 7, and 10 p.i., the right lung was collected for assessment of (D) viral replication by plaque
487 assay. For clinical disease, data are pooled from four independent experiments (n ≤ 70 mice/group).
488 For viral replication, data are pooled from two independent experiments (n = 10 mice/group). Data are
489 expressed as mean ± SEM. Significant results were determined by two-way mixed ANOVA (* $p \leq$
490 0.05, ** $p \leq 0.01$, *** $p \leq 0.001$, **** $p \leq 0.0001$).

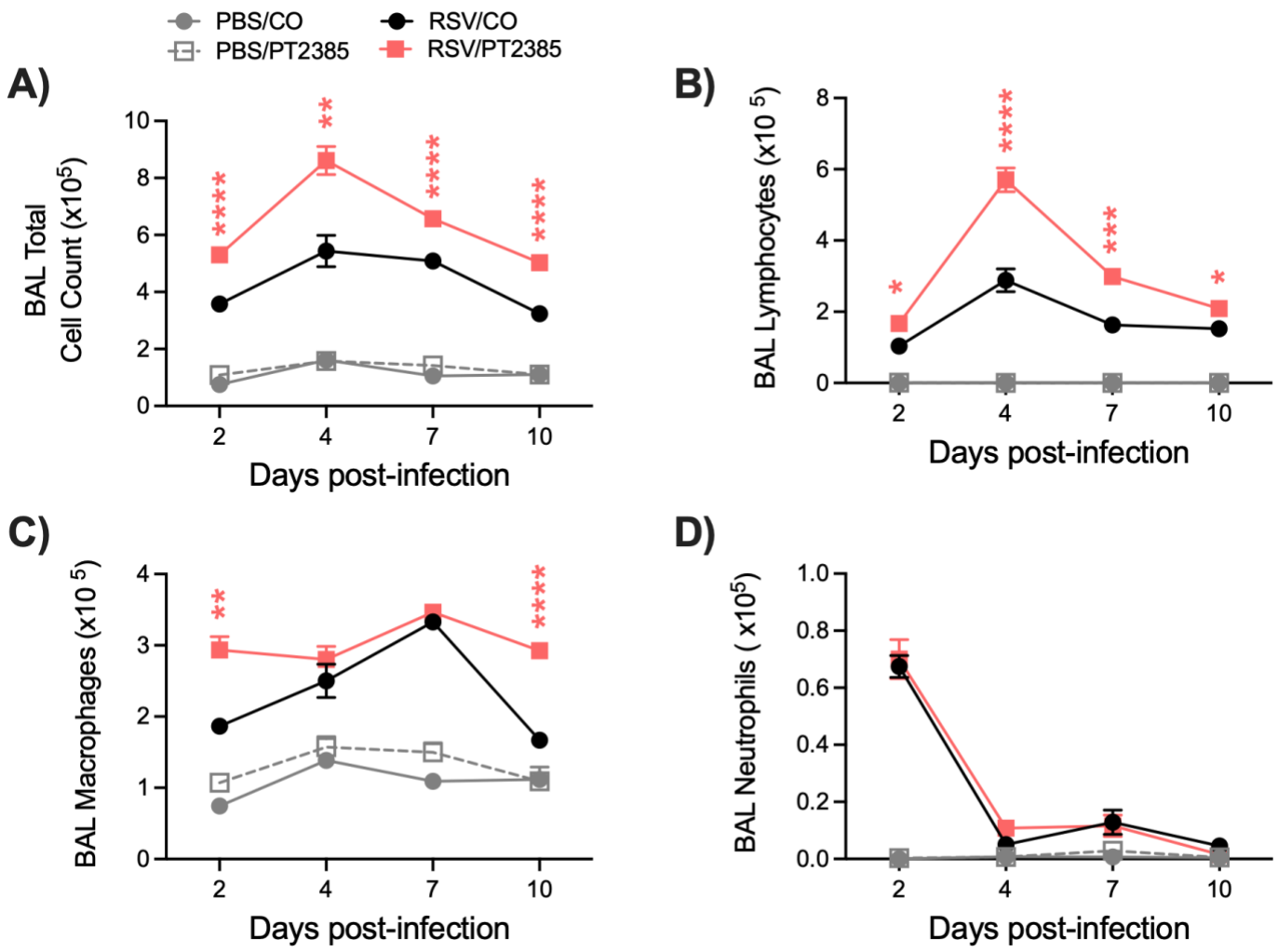

491 **Figure 7.** *Differential cell count of the BAL fluid following HIF-2α inhibition during RSV infection.*
492 At days 2, 4, 7, and 10 p.i., BAL fluid was collected and used to obtain (A) total cell counts, as well as
493 differential cell counts consisting of (B) lymphocytes, (C) macrophages, and (D) neutrophils. Data are
494 pooled from two independent experiments (n ≤ 15 mice/group). Data are expressed as mean ± SEM.
495 Significant results were determined by mixed-effects analysis (* $p \leq 0.05$, ** $p \leq 0.01$, *** $p \leq 0.001$,
496 **** $p \leq 0.0001$).

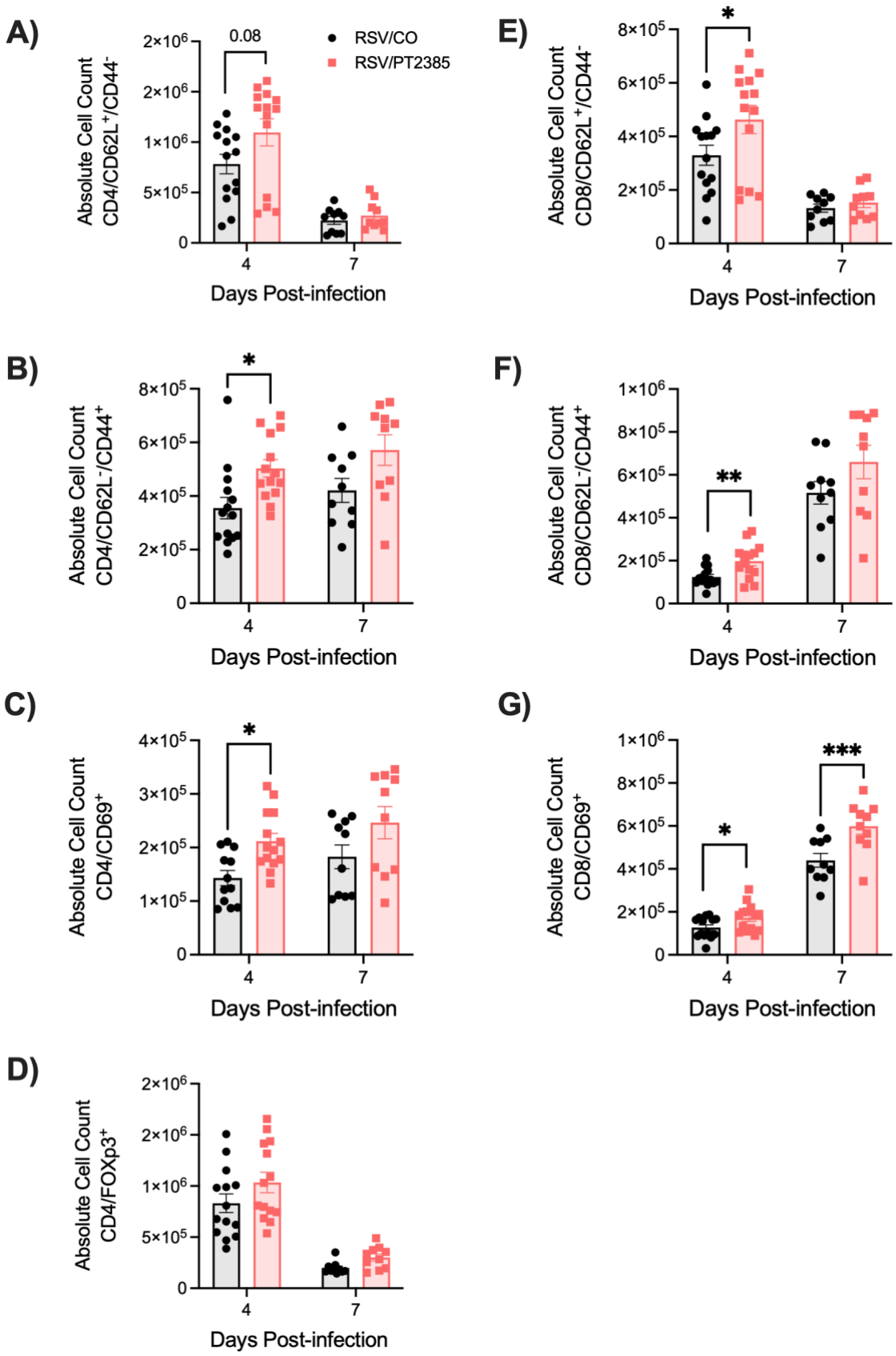
A)
Absolute Cell Count CD4/CD62L+/CD44-
0.08
RSV/CO
RSV/PT2385
Days Post-infection
B)
Absolute Cell Count CD4/CD62L-/CD44+
*
Days Post-infection
C)
Absolute Cell Count CD4/CD69+
*
Days Post-infection
D)
Absolute Cell Count CD4/FOXp3+
Days Post-infection
E)
Absolute Cell Count CD8/CD62L+/CD44-
*
Days Post-infection
F)
Absolute Cell Count CD8/CD62L-/CD44+
**
Days Post-infection
G)
Absolute Cell Count CD8/CD69+
*
***
Days Post-infection

Figure 8. *Assessment of $CD4^+$ and $CD8^+$ T-cells following HIF-2α inhibition during RSV infection.* Whole lung tissue was collected at peak RSV replication and a timepoint of viral clearance, days 4 and 7 p.i., respectively. Single cell suspension was prepared, stained with live/dead cell dye and fluorochrome-conjugated antibodies, and acquired by flow cytometry. Data were analyzed for (A) $CD4^+$ naive cells, (B) $CD4^+$ effector cells, (C) active $CD4^+$ cells, (D) $CD4^+$ Treg cells, (E) $CD8^+$ naive cells, (F) $CD8^+$ effector cells, and (G) active $CD8^+$ cells. Black circle = RSV/CO and pink square = RSV/PT2385. Data are pooled from three independent experiments for day 4 ($n \leq 15$ mice/group) and two independent experiments for day 7 ($n = 10$ mice/group). Data are expressed as mean ± SEM. Significant results were determined by a two-way mixed ANOVA (* $p \leq 0.05$, ** $p \leq 0.01$, *** $p \leq 0.001$).

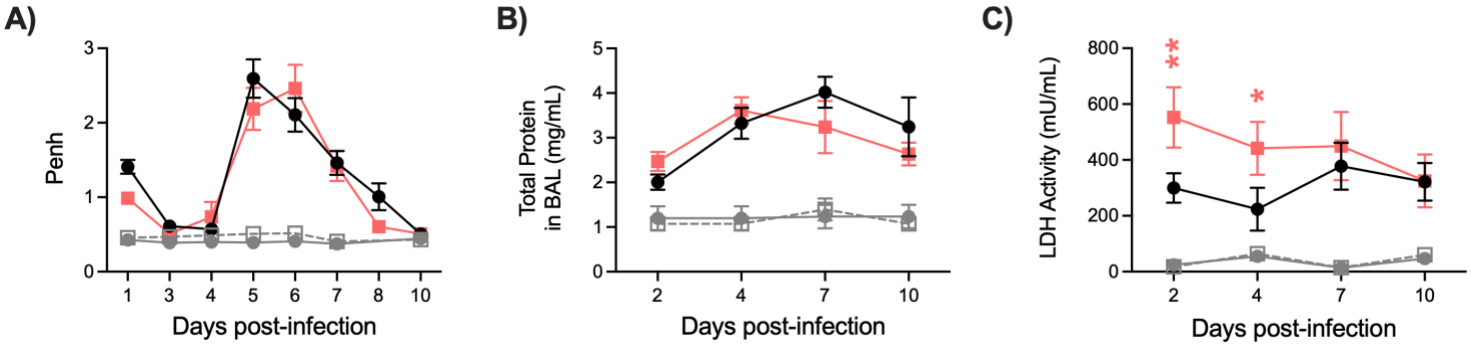

Figure 9. *Assessment of airway function following HIF-2α inhibition during RSV infection.* (A) Bronchoconstriction, represented by baseline Penh, was measured by plethysmography. Using BAL fluid collected at days 2, 4, 7, and 10 p.i., (B) total protein and (C) LDH were measured. For bronchoconstriction, data are pooled from three independent experiments ($n \leq 25$ mice/group). For total protein and LDH, data are pooled from two independent experiments ($n \leq 10$ mice/group). Data are expressed as mean ± SEM. Significant results were determined by two-way mixed ANOVA (* $p \leq 0.05$, ** $p \leq 0.01$).

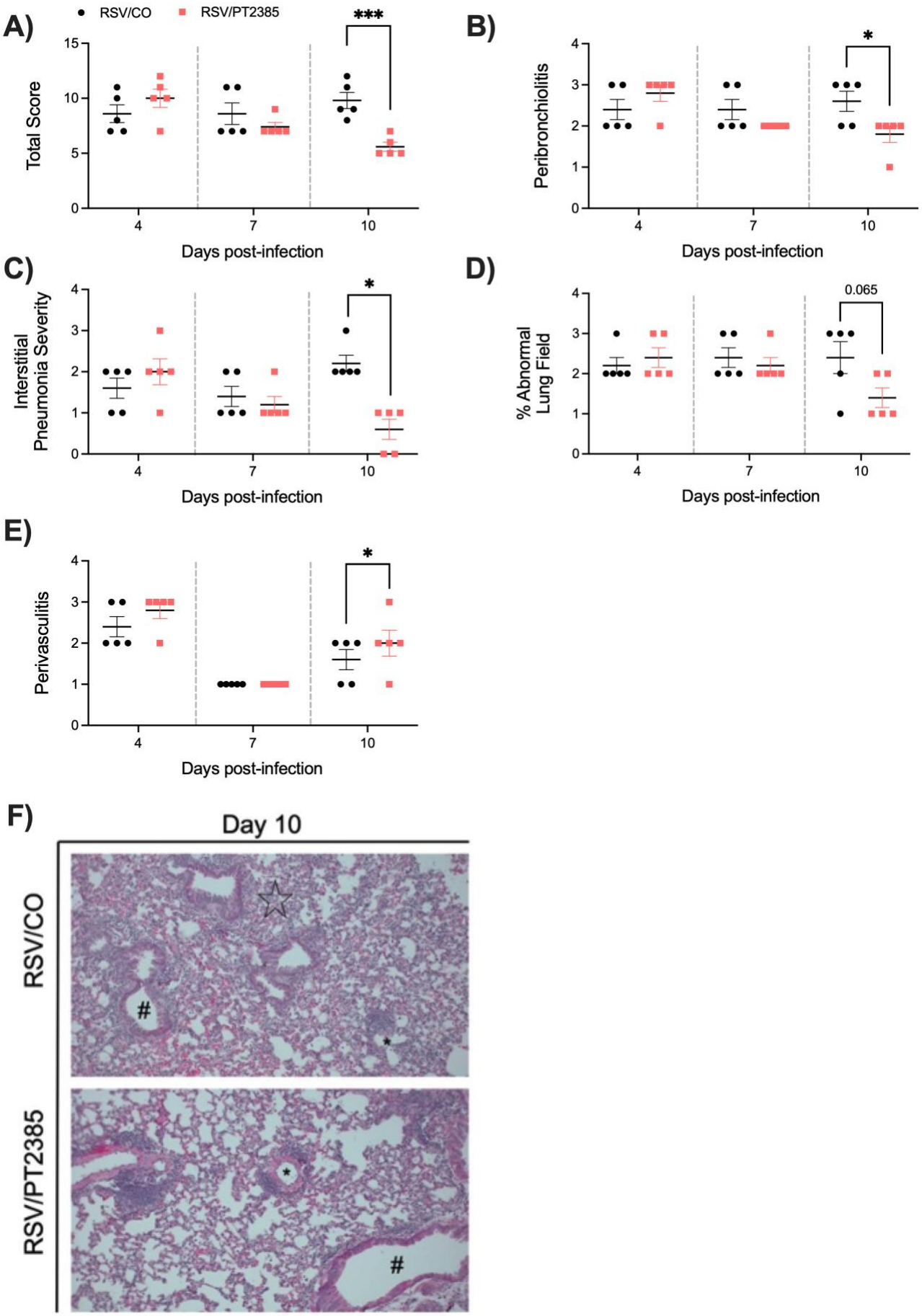
A)
RSV/CO
RSV/PT2385
***
Total Score
Days post-infection
B)
*
Peribronchiolitis
Days post-infection
C)
*
Interstitial Pneumonia Severity
Days post-infection
D)
0.065
% Abnormal Lung Field
Days post-infection
E)
*
Perivasculitis
Days post-infection
F)
Day 10
RSV/CO
RSV/PT2385
#
*

Figure 10. *Histopathological scoring of lung tissue following HIF-2α inhibition during RSV infection.* At days 4, 7, and 10 p.i., the left lung was collected from RSV infected mice that had received CO or PT2385 and subjected to FFPE. Cuts of lung tissue were stained with H&E and observed under a microscope at 10X magnification. The (A) total score was calculated, consisting of scores for (B) peribronchiolitis, (C) interstitial pneumonia, (D) percent abnormal lung field, and (E) perivasculitis. Representative images are shown in (F). Perivasculitis is indicated by an asterisk. Peribronchiolitis is indicated by the hash sign. Interstitial pneumonia is indicated by the black star. No interstitial pneumonia present in RSV/PT2385 on day 10. Data are representative of one independent experiment (n = 5 mice/group). Data are expressed as mean ± SEM. Significant results were determined by an unpaired student's t-test (* $p \leq 0.05$, *** $p \leq 0.001$).

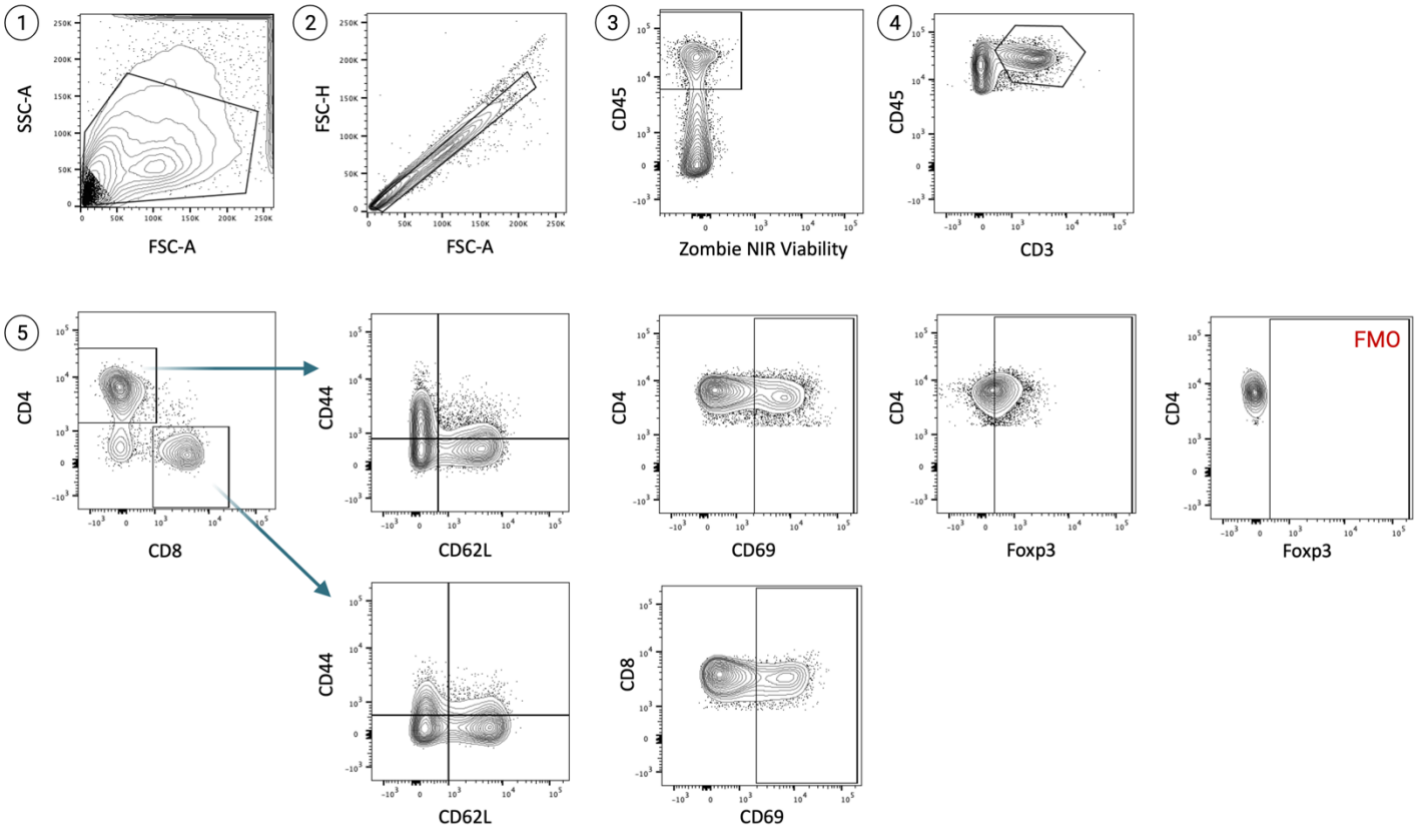

Figure S1. *Schematic for analysis of CD4+ and CD8+ T-cells by flow cytometry.* At days 4 and 7 p.i., whole lung tissue was collected from the respective groups. Single cell suspension was prepared, stained with live/dead cell dye and fluorochrome-conjugated antibodies, followed by flow cytometric analysis. T cells were gated on $CD45^{+}CD3^{+}$ first, then further gated on $CD4^{+}$ and $CD8^{+}$ subpopulations. Naïve and effector T cells were gated on $CD44^{-}CD62L^{+}$ and $CD44^{+}CD62L^{-}$ respectively. CD69 was used as an early activation marker of T cells. Tregs were defined as $CD45^{+}CD3^{+}CD4^{+}Foxp3^{+}$ and gated according to an FMO control.

12 References

1. Shi, T., et al., *Global, regional, and national disease burden estimates of acute lower respiratory infections due to respiratory syncytial virus in young children in 2015: a systematic review and modelling study.* The Lancet, 2017. **390**(10098): p. 946-958.
2. Kampmann, B., et al., *Bivalent Prefusion F Vaccine in Pregnancy to Prevent RSV Illness in Infants.* New England Journal of Medicine, 2023. **388**(16): p. 1451-1464.
3. Papi, A., et al., *Respiratory Syncytial Virus Prefusion F Protein Vaccine in Older Adults.* New England Journal of Medicine, 2023. **388**(7): p. 595-608.
4. Muller, W.J., et al., *Nirsevimab for Prevention of RSV in Term and Late-Preterm Infants.* New England Journal of Medicine, 2023. **388**(16): p. 1533-1534.
5. Thaker, S.K., J. Ch'ng, and H.R. Christofk, *Viral hijacking of cellular metabolism.* BMC Biology, 2019. **17**(1): p. 59.
6. Reyes, A., et al., *Contribution of hypoxia inducible factor-1 during viral infections.* Virulence, 2020. **11**(1): p. 1482-1500.
7. Huang, R., et al., *Hypoxia and viral infectious diseases.* JCI Insight, 2021. **6**(7).
8. Semenza, G.L., *Pharmacologic Targeting of Hypoxia-Inducible Factors.* Annual Review of Pharmacology and Toxicology, 2019. **59**(1): p. 379-403.
9. Reyes, A., et al., *Impact of Hypoxia over Human Viral Infections and Key Cellular Processes.* Int J Mol Sci, 2021. **22**(15).
10. Brahimi-Horn, M.C. and J. Pouysségur, *HIF at a glance.* Journal of Cell Science, 2009. **122**(8): p. 1055-1057.
11. Infantino, V., et al., *Cancer Cell Metabolism in Hypoxia: Role of HIF-1 as Key Regulator and Therapeutic Target.* International Journal of Molecular Sciences, 2021. **22**(11): p. 5703.
12. Koh, M.Y. and G. Powis, *Passing the baton: the HIF switch.* Trends Biochem Sci, 2012. **37**(9): p. 364-72.
13. Zhang, P., et al., *Hypoxia-Inducible Factor 3 Is an Oxygen-Dependent Transcription Activator and Regulates a Distinct Transcriptional Response to Hypoxia.* Cell Reports, 2014. **6**(6): p. 1110-1121.
14. Downes, N.L., et al., *Differential but Complementary HIF1alpha and HIF2alpha Transcriptional Regulation.* Mol Ther, 2018. **26**(7): p. 1735-1745.
15. Morris, D.R., et al., *HIF-1α Modulates Core Metabolism and Virus Replication in Primary Airway Epithelial Cells Infected with Respiratory Syncytial Virus.* Viruses, 2020. **12**(10).
16. Ivanciuc, T., et al., *Micro-CT Features of Lung Consolidation, Collagen Deposition and Inflammation in Experimental RSV Infection Are Aggravated in the Absence of Nrf2.* Viruses, 2023. **15**(5).
17. Morris, D.R., et al., *Selective Blockade of TNFR1 Improves Clinical Disease and Bronchoconstriction in Experimental RSV Infection.* Viruses, 2020. **12**(10).
18. Morris, D., et al., *Antiviral and Immunomodulatory Activity of Silver Nanoparticles in Experimental RSV Infection.* Viruses, 2019. **11**(8).

19. Qu, Y., et al., *SARS-CoV-2 Inhibits NRF2-Mediated Antioxidant Responses in Airway Epithelial Cells and in the Lung of a Murine Model of Infection.* Microbiol Spectr, 2023. **11**(3): p. e0037823.

20. Russell, C.D., et al., *The Human Immune Response to Respiratory Syncytial Virus Infection.* 2017. **30**(2): p. 481-502.

21. De, C., et al., *Human T cells efficiently control RSV infection.* JCI Insight, 2023. **8**(11).

22. McGinley, J., et al., *A Systematic Review and Meta-analysis of Animal Studies Investigating the Relationship Between Serum Antibody, T Lymphocytes, and Respiratory Syncytial Virus Disease.* The Journal of Infectious Diseases, 2021. **226**(Supplement_1): p. S117-S129.

23. Shimoda, L.A. and G.L. Semenza, *HIF and the lung: role of hypoxia-inducible factors in pulmonary development and disease.* Am J Respir Crit Care Med, 2011. **183**(2): p. 152-6.

24. Wicks, E.E. and G.L. Semenza, *Hypoxia-inducible factors: cancer progression and clinical translation.* J Clin Invest, 2022. **132**(11).

25. Lee, J.W., et al., *Hypoxia signaling in human diseases and therapeutic targets.* Experimental & Molecular Medicine, 2019. **51**(6): p. 1-13.

26. Jacoby, J.J., et al., *Treatment with HIF-1alpha antagonist PX-478 inhibits progression and spread of orthotopic human small cell lung cancer and lung adenocarcinoma in mice.* J Thorac Oncol, 2010. **5**(7): p. 940-9.

27. Xu, L., et al., *Antitumor effect of the selective hypoxia-inducible factor-1 inhibitors echinomycin and PX-478 on uterine fibroids.* F S Sci, 2022. **3**(2): p. 187-196.

28. Welsh, S., et al., *Antitumor activity and pharmacodynamic properties of PX-478, an inhibitor of hypoxia-inducible factor-1α.* Molecular Cancer Therapeutics, 2004. **3**(3): p. 233-244.

29. Palayoor, S.T., et al., *PX-478, an inhibitor of hypoxia-inducible factor-1α, enhances radiosensitivity of prostate carcinoma cells.* International Journal of Cancer, 2008. **123**(10): p. 2430-2437.

30. Xu, K., et al., *Hypoxia Induces Drug Resistance in Colorectal Cancer through the HIF-1alpha/miR-338-5p/IL-6 Feedback Loop.* Mol Ther, 2019. **27**(10): p. 1810-1824.

31. Abe, Y., et al., *Tumor protein D52 is upregulated in oral squamous carcinoma cells under hypoxia in a hypoxia-inducible-factor-independent manner and is involved in cell death resistance.* Cell & Bioscience, 2021. **11**(1): p. 122.

32. Tibes, R., et al., *Results from a phase I, dose-escalation study of PX-478, an orally available inhibitor of HIF-1α.* Journal of Clinical Oncology, 2010. **28**(15_suppl): p. 3076-3076.

33. Tibes, R., et al., *Results from a phase I, dose-escalation study of PX-478, an orally available inhibitor of HIF-1α.* Journal of Clinical Oncology, 2010. **28**(15_suppl): p. 3076-3076.

34. Villa-Roel, N., et al., *Hypoxia inducible factor 1α inhibitor PX-478 reduces atherosclerosis in mice.* Atherosclerosis, 2022. **344**: p. 20-30.

35. Sun, K., et al., *Selective Inhibition of Hypoxia-Inducible Factor 1α Ameliorates Adipose Tissue Dysfunction.* Molecular and Cellular Biology, 2013. **33**(5): p. 904-917.

36. Ilegems, E., et al., *HIF-1a inhibitor PX-478 preserves pancreatic beta cell function in diabetes.* Science Translational Medicine, 2022. **14**(638): p. eaba9112.

37. Taylor, C.T. and C.C. Scholz, *The effect of HIF on metabolism and immunity.* Nature Reviews Nephrology, 2022. **18**(9): p. 573-587.

38. Martín-Vicente, M., et al., *Metabolic changes during respiratory syncytial virus infection of epithelial cells.* PLoS One, 2020. **15**(3): p. e0230844.

39. Connelly, A.R., et al., *Metabolic Reprogramming of Nasal Airway Epithelial Cells Following Infant Respiratory Syncytial Virus Infection.* Viruses, 2021. **13**(10).

40. Li, M., et al., *Respiratory Syncytial Virus Replication Is Promoted by Autophagy-Mediated Inhibition of Apoptosis.* Journal of Virology, 2018. **92**(8): p. 10.1128/jvi.02193-17.

41. Chiok, K., et al., *Human Respiratory Syncytial Virus NS2 Protein Induces Autophagy by Modulating Beclin1 Protein Stabilization and ISGylation.* mBio, 2022. **13**(1): p. e0352821.

42. Shuchi, S., et al., *Modulation of autophagy and mTOR signaling pathway genes in respiratory epithelium by respiratory syncytial virus (RSV) in children suffering from acute lower respiratory tract infections.* Journal of Medical Virology, 2023. **95**(3): p. e28666.

43. Zhang, H., et al., *Mitochondrial autophagy is an HIF-1-dependent adaptive metabolic response to hypoxia.* J Biol Chem, 2008. **283**(16): p. 10892-903.

44. Zhou, J., et al., *Hypoxia-inducible factor-1α-dependent autophagy plays a role in glycolysis switch in mouse granulosa cells†.* Biology of Reproduction, 2018. **99**(2): p. 308-318.

45. McGettrick, A.F. and L.A.J. O'Neill, *The Role of HIF in Immunity and Inflammation.* Cell Metab, 2020. **32**(4): p. 524-536.

46. Bhat, R., M.A. Farrag, and F.N. Almajhdi, *Double-edged role of natural killer cells during RSV infection.* Int Rev Immunol, 2020. **39**(5): p. 233-244.

47. Bergeron, H.C. and R.A. Tripp, *Immunopathology of RSV: An Updated Review.* Viruses, 2021. **13**(12): p. 2478.

48. Luckheeram, R.V., et al., *$CD4^+$T cells: differentiation and functions.* Clin Dev Immunol, 2012. **2012**: p. 925135.

49. Schmidt, M.E. and S.M. Varga, *Cytokines and CD8 T cell immunity during respiratory syncytial virus infection.* Cytokine, 2020. **133**: p. 154481.

50. Hsu, T.-S., et al., *HIF-2α is indispensable for regulatory T cell function.* Nature Communications, 2020. **11**(1): p. 5005.

51. Ajouaou, Y., et al., *The oxygen sensor prolyl hydroxylase domain 2 regulates the in vivo suppressive capacity of regulatory T cells.* eLife, 2022. **11**: p. e70555.

52. Ahmad, T., et al., *Hypoxia response in asthma: differential modulation on inflammation and epithelial injury.* Am J Respir Cell Mol Biol, 2012. **47**(1): p. 1-10.

53. Dewitz, C., et al., *Hypoxia-inducible factor-1α inhibition modulates airway hyperresponsiveness and nitric oxide levels in a BALB/c mouse model of asthma.* Clinical Immunology, 2017. **176**: p. 94-99.

54. Pan, S., S. Conaway, Jr., and D.A. Deshpande, *Mitochondrial regulation of airway smooth muscle functions in health and pulmonary diseases.* Arch Biochem Biophys, 2019. **663**: p. 109-119.

55. Bartman, C.M., et al., *Cellular clocks in hyperoxia effects on [Ca2+]i regulation in developing human airway smooth muscle.* American Journal of Physiology-Lung Cellular and Molecular Physiology, 2021. **320**(3): p. L451-L466.

56. Evans, C.E., *Hypoxia-Inducible Factor Signaling in Inflammatory Lung Injury and Repair*. Cells, 2022. **11**(2).

57. Rodriguez, D., et al., *Hypoxia Pathway Proteins and Their Impact on the Blood Vasculature.* International Journal of Molecular Sciences, 2021. **22**(17): p. 9191.